ELSEVIER

Biochimica et Biophysica Acta 1468 (2000) 293–303

BIOCHIMICA ET BIOPHYSICA ACTA
BBA

www.elsevier.com/locate/bba

Fourier transform infrared spectroscopy and differential scanning calorimetry studies of fatty acid homogeneous ceramide 2

Hui-Chen Chen [a], Richard Mendelsohn [a], Mark E. Rerek [b], David J. Moore [b,*]

[a] *Rutgers University, Department of Chemistry, 73 Warren Street, Newark, NJ 07102, USA*
[b] *International Specialty Products, 1361 Alps Road (1-012), Wayne, NJ 07470, USA*

Received 28 March 2000; received in revised form 15 June 2000; accepted 29 June 2000

Abstract

Ceramides provide a major component of the barrier function of skin. An understanding of barrier organization requires a detailed characterization of ceramide phase behavior and molecular interactions. Toward this end, Fourier transform infrared (FTIR) and differential scanning calorimetry (DSC) studies of ceramide 2 analogues (non-hydroxylated fatty acid *N*-acyl sphingosines) of specific chain lengths (C_{14}, C_{16}, C_{18}, C_{20}) are presented. In addition, the molecular interactions of the individual chains in each molecule are elucidated through thermotropic FTIR studies of derivatives possessing perdeuterated fatty acid chains. DSC data showed a much smaller chain length variation (for the C_{16}, C_{18}, C_{20} derivatives) in the main order-disorder transition temperature (approx. 93 ± 1°C) than is observed in the corresponding series of phosphatidylcholines, consistent with minimal ceramide hydration. The temperature dependence of the methylene stretching and scissoring modes revealed a solid-solid phase transition at 20–25°C below the main order-disorder transition accompanied by chain packing alterations from orthorhombic → hexagonal subcells. The chain packing transition was accompanied by enhanced penetration of water into the polar region. This was deduced from the temperature dependence of the amide I and II modes, which provide direct evidence for H → D exchange. The CD_2 scissoring mode splitting of the deuterated fatty acid constituent of the C_{16}, C_{18}, C_{20} chains revealed preferential segregation of microdomains (3–5 chains) of this species within the orthorhombic phase. In contrast, the sphingosine base chains appeared to be sufficiently separated so as to inhibit interchain vibrational coupling between them. FTIR spectroscopy provides a convenient means for characterizing domain formation, chain packing, and hydration sites of these phases, which are highly ordered under physiological conditions.

Keywords: Skin; Lipid barrier; Conformational order

1. Introduction

The thin outer layer of human skin consists of terminally differentiated anucleated cells (corneocytes) within a lamellar matrix of bilayer lipids. This outer layer of skin, the stratum corneum (SC), provides the human body with a permeability barrier which prevents penetration of most biological and chemical agents into the body [1]. Moreover, the SC prevents unregulated water loss from the body through the skin and thus plays a crucial role in human physiology by maintaining water homeostasis [2]. The major components of the extracellular matrix of the SC are three families of lipids: ceramides,

* Corresponding author. Fax: (973) 6284007;
E-mail: dmoore@ispcorp.com

0005-2736/00/$ – see front matter
PII: S0005-2736(00)00271-6

free fatty acids, and sterols [3–5]. The ceramides consist of at least seven different species with a wide range of long to very long fatty acid chains. The free fatty acids are saturated, primarily C_{20} to C_{30}, while the sterol component is mostly cholesterol, cholesterol sulfate, and cholesterol esters [6–8]. There have been a few calorimetry [9–11], X-ray [12–15], and NMR [16–19] studies of skin lipids; however, overall there are relatively few published studies on the phase behavior and physical chemistry of SC lipids and particularly, hydrated ceramides. A consistent finding of the published biophysical studies is that lipid organization in the SC is unlike that in other membranes, particularly in its highly ordered nature. This is appropriate for the barrier function of the SC lipids as well as with their chemical structure, i.e., long hydrocarbon chains and small polar headgroups.

Our laboratories are pursuing an understanding of the phase behavior and molecular organization of SC lipids [20–24]. Such studies are required particularly since the phase behavior of ceramides is significantly different from phospholipids and other more widely studied biological membrane lipids. To date, most reports on ceramides have utilized material isolated from animal sources such as bovine brain or pig skin, which naturally contain a distribution of amide-linked fatty acid chains and well as sphingosine base chains. The current investigation utilizes synthetic non-hydroxylated fatty acid *N*-acyl sphingosines (ceramide 2) with specified chain lengths (C_{14}, C_{16}, C_{18} and C_{20}). In addition, the use of deuterated derivatives of these chains permits the separate and simultaneous evaluation of the conformational order and packing properties of the sphingosine base chains and of the amide linked fatty acid chains in each derivative. Substitution of ^2H_2O for H_2O buffer permits detailed analysis of the headgroup structure and interactions through direct spectroscopic monitoring of the ceramide amide I and II modes. The combined use of infrared (IR) spectroscopy and differential scanning calorimetry (DSC) provides a detailed investigation of ceramide 2 phase behavior without the ambiguity and complications present with a mixture of lipid chain lengths.

Ceramide 2, as one of the most abundant ceramides in the human skin barrier, plays a critical role in the overall lipid matrix organization of the stratum corneum. The current study of synthetic ceramide 2 derivatives/analogues provides a detailed picture of the molecular level organization and phase behavior of hydrated ceramide 2 under highly controlled conditions. This picture will add to our understanding of the contribution ceramide 2 makes to the cohesion, integrity, and function of the lipid skin barrier.

2. Experimental section

2.1. Materials

A series of synthetic non-hydroxylated fatty acid ceramides (*N*-acyl-D-*erythro*-sphingosine) representing human SC ceramide 2, and comprising amide linked fatty acid chains of tetradecanoic acid (C14-Cer), hexadecanoic acid (C16-Cer), octadecanoic acid (C18-Cer), and eicosanoic acid (C20-Cer) were purchased from Northern Lipids (Vancouver, Canada). An equivalent series of ceramides with perdeuterated fatty acid chains were also purchased from the same source. In all cases, the sphingosine chain was a C18 chain with a *trans* 4,5 double bond. The chemical structure of these ceramides is shown in Fig. 1.

2.2. Fourier transform infrared (FTIR) spectroscopy

Ceramide films for FTIR experiments were pre-

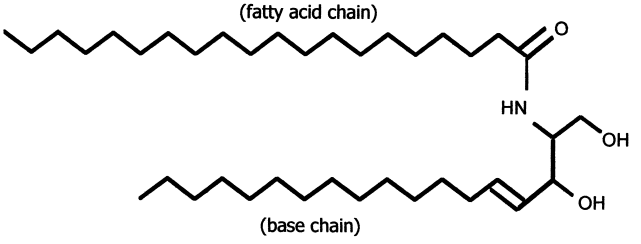

Fatty acid chain composition:	
C14-h_{27}-Cer	C14-d_{27}-Cer
C16-h_{31}-Cer	C16-d_{31}-Cer
C18-h_{35}-Cer	C18-d_{35}-Cer
C20-h_{39}-Cer	C20-d_{39}-Cer

Fig. 1. The chemical structure of ceramide 2 and the various fatty acid chains used in the current study.

pared by evaporation from chloroform solution (2 mg in 200 μl) onto a ZeSe horizontal attenuated total reflection (HATR) crystal mounted in a trough plate and placed in a temperature-controlled, horizontal ATR setup (Spectra-Tech, Shelton, CT). The lipid film was submerged under excess buffer (pH 5.5, 150 mM NaCl, 100 mM citric acid, 4 mM EDTA in H_2O or ^2H_2O) and the trough covered to retard buffer evaporation. FTIR spectra were acquired on a Mattson RS1 spectrometer equipped with a broad band mercury-cadmium telluride (MCT) detector and kept under continuous dry air purge. Spectra were generated by coaddition of 256 interferograms collected at 2 cm^{-1} resolution. IR spectra were acquired at 2°C intervals from 25 to 95°C. IR spectra were analyzed off-line primarily using software written at the National Research Council of Canada. Figures were generated using Sigma Plot 5.0 (SPSS, Chicago, IL).

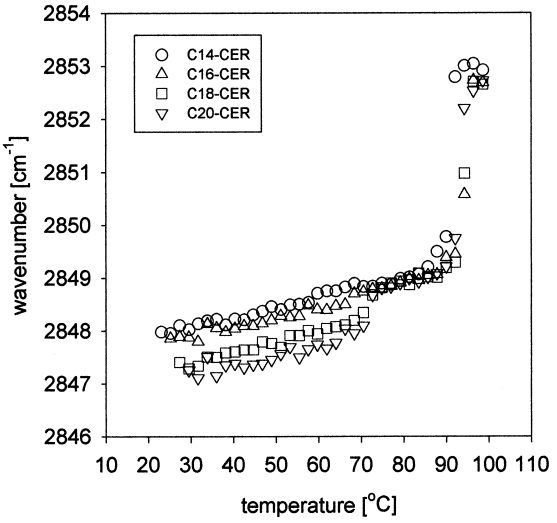

Fig. 2. The temperature dependence of the ν_sCH_2 of hydrated samples of C14-Cer (○), C16-Cer (△), C18-Cer (□) and C20-Cer (▽).

2.3. Differential scanning calorimetry

Hydrated ceramide samples were prepared by first dissolving the ceramides in chloroform and pipetting the appropriate volume into pre-weighed stainless steel pans. Bulk phase $CHCl_3$ was removed under a gentle stream of N_2 gas. The sample was then dried under vacuum overnight, hydrated with 40 μl of H_2O buffer and the pans sealed. All samples were kept at −10°C prior to measurements.

DSC measurements were made with a Perkin-Elmer Pyris-1 DSC differential scanning calorimeter (Norwalk, CT) at heating rates of 1 and 5°C per min. The samples were repeatedly cycled from 25 to 90°C at 5°C/min to ensure uniform hydration, following 1–2 h of equilibration in the instrument. Duplicate runs of the same sample gave onset, midpoint, and completion temperatures reproducible to 1°C. Final thermograms were recorded at a scan rate of 1°C/min. Data were analyzed using Perkin-Elmer Thermal Data Analysis software. The enthalpy was determined from the area under the transition peak by comparison with an indium standard.

3. Results

Fig. 2 shows the thermotropic response of the IR symmetric methylene stretching mode frequency (ν_sCH_2) near 2850 cm^{-1} for C14-Cer, C16-Cer, C18-Cer, and C20-Cer hydrated in ^2H_2O buffer. In all cases the ceramides undergo a phase transition from ordered all-*trans* chains to conformationally disordered chains near 90°C, characterized by an increase of approx. 4 cm^{-1} in ν_sCH_2. It is of interest to note the similarity in transition temperatures for these four molecules, which differ by up to six carbons in fatty acid chain length. Between 20°C and the major chain disordering transition, the ν_sCH_2 frequency of C14-Cer and C16-Cer rises monotonically from approx. 2848 to 2849 cm^{-1}. For C18-Cer and C20-Cer the initial ν_sCH_2 frequency of approx. 2847 cm^{-1} monotonically increases to approx. 2848 cm^{-1} then undergoes a sharp 1 cm^{-1} transition at approx. 70°C. For all ceramides, ν_sCH_2 remains at approx. 2849 cm^{-1} from 73°C until the onset of the highly cooperative chain melting transition at 90°C. All experiments were repeated several times in both H_2O and ^2H_2O buffers and all transition temperatures were reproducible to within 1–2°C. Small variations in the absolute value of ν_sCH_2 were observed such that the lowest (low temperature) value for this parameter was sometimes observed for C18-Cer rather than C20-Cer. However, C18-Cer and C20-Cer frequencies were always grouped together and were lower than C16-Cer and C14-Cer, suggesting

a more ordered, tightly packed, chain organization for the longer chain fatty acid ceramides. The structural origin of the low temperature transition is confirmed from studies of the $\nu_s CH_2$ mode as noted below and as discussed previously [21].

Perdeuteration of the ceramide fatty acid chains permits the thermotropic response, conformational order, and packing behavior of the ceramide fatty acid and base chains to be probed directly and individually. The $\nu_s CH_2$ frequencies for the base chains of these hydrated ceramides are plotted in Fig. 3A. The conformational behavior of the base chain, which is the same length in all these ceramides, is clearly influenced by the fatty acid chain length. At low temperatures, the base chains of the d_{35}C18-Cer and d_{39}C20-Cer are more ordered than the d_{31}C16-Cer and d_{27}C14-Cer. As with the fully proteated molecules, there is clear evidence of a solid-solid transition at temperatures prior to the main phase transition. Both d_{27}C14-Cer and d_{31}C16-Cer undergo this process at 63°C as indicated by a frequency increase

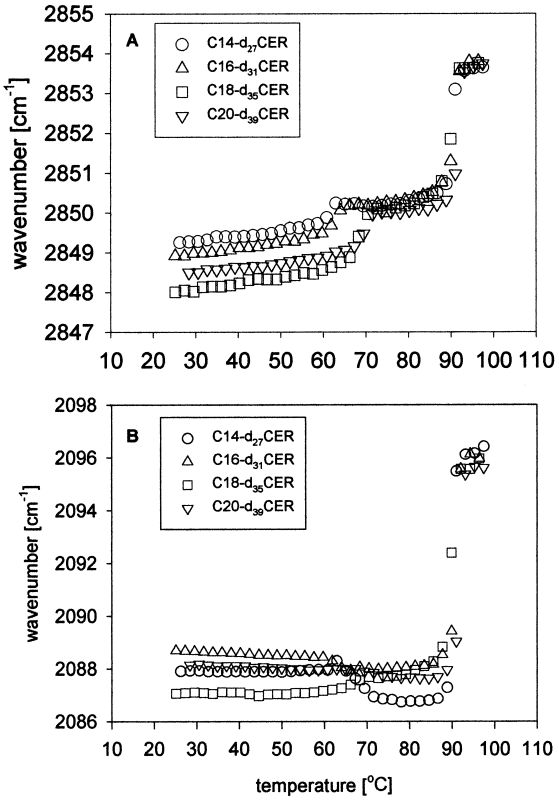

Fig. 3. The temperature dependence of $\nu_s CH_2$ from the base chains (A) and $\nu_s CD_2$ from the fatty acid chains (B) of d_{27}C14-Cer (○), d_{31}C16-Cer (△), d_{35}C18-Cer (□) and d_{39}C20-Cer (▽).

in $\nu_s CH_2$ from 2849 to 2850 cm^{-1} while the d_{35}C18-Cer and d_{39}C20-Cer derivatives exhibit their solid-solid transition at 70°C characterized by an increase in $\nu_s CH_2$ from approx. 2848.5 to 2850 cm^{-1}. The base chains in all the ceramide derivatives undergo their main order-disorder transitions at 90–93°C. It is noted that above 70°C, the conformational behavior of the base chain in all four ceramide molecules is equivalent. However, at temperatures below this value (which are of physiological interest for understanding the SC barrier function) the properties of the base chain are clearly influenced by the length of the fatty acid chain. Thus, in ceramides with longer fatty acid chains (e.g., d_{35}C18-Cer and d_{39}C20-Cer) the base chains exist in a more tightly packed structure (see Section 4), as indicated by the lower value of $\nu_s CH_2$. The conformational behavior of the ceramide fatty acid chains is monitored via the thermotropic response of $\nu_s CD_2$. This is plotted as a function of temperature for all four ceramide molecules in Fig. 3B. The most intriguing result is that $\nu_s CD_2$ for d_{27}C14-Cer and d_{31}C16-Cer *decreases* in value by approx. 1.5 and 0.5 cm^{-1} at 65°C, respectively, i.e., where the solid-solid transition is observed in the base chains in Fig. 3A. This phenomenon is unexpected as methylene frequencies usually increase with temperature as intramolecular conformational disorder increases. The longer chain ceramides, d_{35}C18-Cer and d_{39}C20-Cer, exhibit less clear-cut behavior. The $\nu_s CD_2$ of the fatty acid chain of d_{35}C18-Cer increases slightly from 60 to 70°C whereas $\nu_s CD_2$ of d_{39}C20-Cer does not undergo any sharp change, but rather, monotonically decreases in frequency by < 0.5 cm^{-1} from 60°C to 80°C. The deuterated fatty acid chains and proteated base chains of all the ceramides then undergo their major transition from conformationally ordered to conformationally disordered chains at about 92°C. The detailed, chain specific, information in Fig. 3 illustrates the utility of isotope labeling in biophysical IR spectroscopy (see Section 4).

Qualitative information about rates of acyl chain motion are available from the thermotropic behavior of the linewidths of $\nu_s CH_2$ for the fully proteated and specific fatty acid perdeuterated species. The linewidth data for the four fully proteated molecules and for the fatty acid deuterated derivatives are shown in Fig. 4A and B respectively. The linewidths

of all the base chains are less than the linewidths measured for both chains in Fig. 4A. This probably arises from inhomogeneous broadening since the base chains have slightly different CH_2 stretching frequencies than the fatty acid chains in the fully proteated derivatives (compare Figs. 2 and 3), leading to a broadened overall band contour in Fig. 4A. More interesting is the thermotropic behavior of the base chain linewidth of the d_{27}C14-Cer derivative. The width of the $\nu_s CH_2$ mode in the d_{27}C14-Cer derivative is much larger than for the other three derivatives (Fig. 4B) and suggests increased rates of motion for the sphingosine chain in this instance.

The transition temperatures of the four fully proteated ceramides were also measured with DSC. Thermograms from the hydrated lipid films are plotted in Fig. 5. Typical T_m values were 86.3, 94.1, 92.7, and 92.9°C for C14-Cer, C16-Cer, C18-Cer, and C20-Cer, respectively, while the calculated ΔH values

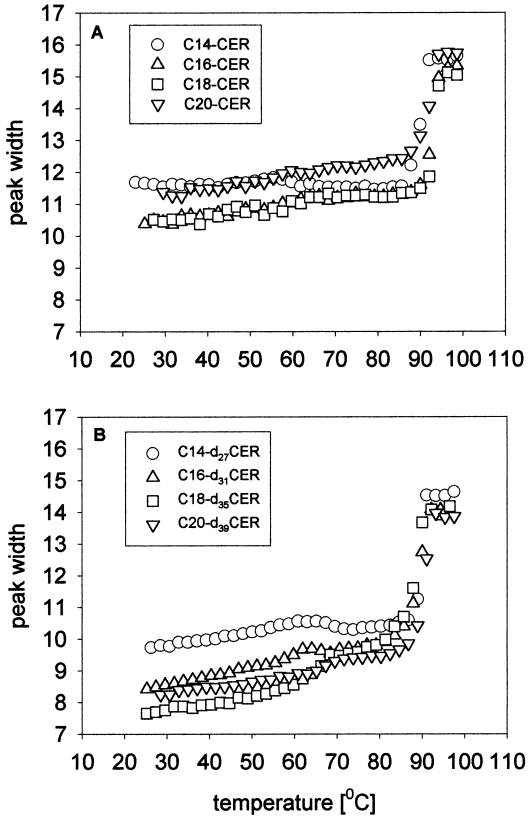

Fig. 4. Linewidths (full widths at half-height) for the CH_2 symmetric stretching vibration for (A) C14-Cer (○), C16-Cer (△), C18-Cer (□) and C20-Cer (▽) and (B) d_{27}C14-Cer (○), d_{31}C16-Cer (△), d_{35}C18-Cer (□) and d_{39}C20-Cer (▽).

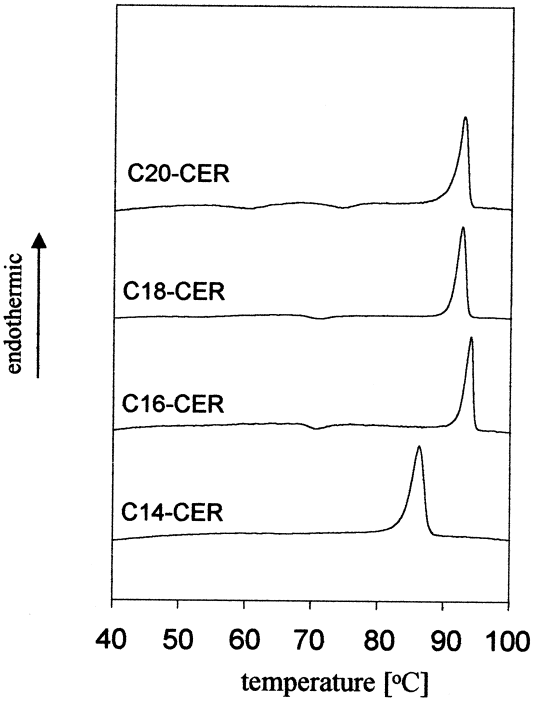

Fig. 5. DSC thermograms of hydrated C14-Cer, C16-Cer, C18-Cer and C20-Cer. The heating rates were 1°C/min.

were 59.0, 73.2, 74.9, 71.8 kJ/mol, respectively. The C14-Cer consistently melted several degrees lower than the other ceramides, although the magnitude of this effect depended somewhat on the sample preparation method. When the ceramides were hydrated from a dried powder (not a film) the T_m of C14-Cer was much closer to the other ceramides again around 92°C. The DSC data are reported for the hydrated film method as that corresponds to the method used to prepare the IR samples. The DSC transition temperatures show very good agreement with those observed in the IR experiments.

In addition to monitoring chain conformational order (i.e., intramolecular behavior), FTIR spectroscopy is convenient for determination of intermolecular chain packing arrangements [25,26]. These are monitored via the methylene bending (δCH_2 and δCD_2) modes. In Fig. 6 the temperature dependence of the δCH_2 spectral region (1450–1480 cm^{-1}) is shown for proteated C14-Cer and C20-Cer. For all the ceramides, including C16-Cer and C18-Cer for which data are not shown, the broad nature of the δCH_2 spectral band at low temperatures indicates the presence of at least two, and probably three under-

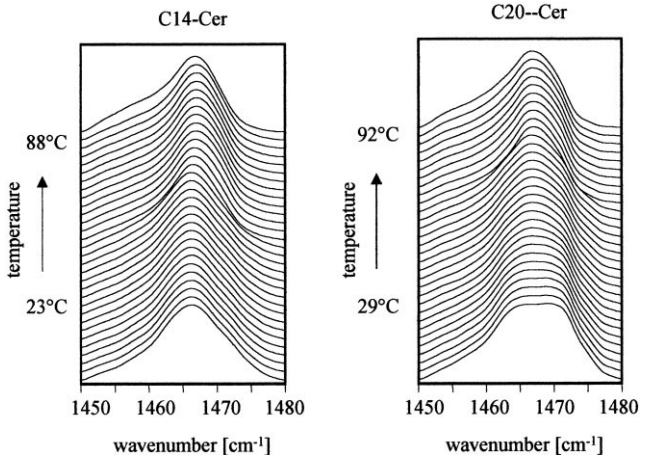

Fig. 6. Original spectra showing the δCH_2 spectral region of hydrated C14-Cer and C20-Cer as a function of temperature. Spectra were acquired at approx. 2°C intervals over the indicated ranges. Spectra are offset on the vertical scale for clarity. Note the reduced (or absent) splitting in the C14-Cer derivative.

lying modes. The band positions can be estimated from second derivative spectra (not shown). In all cases, a central component at 1468 cm^{-1}, characteristic of hexagonally packed chains, and two bands from the orthorhombically packed chains at approx. 1465 and 1472 cm^{-1} are observed, although this is less evident for C14-Cer compared to the others. For the derivatives with the three longest chains, the bandwidth of the entire contour decreases at 65°C, corresponding to a breakdown of orthorhombic perpendicular chain packing (this is also evident in the stretching mode behavior in Figs. 2 and 3). The packing interactions of the individual chains are revealed by analyzing separately the δCH_2 and δCD_2 spectral regions of d_{27}C14-Cer and d_{39}C20-Cer, as shown in Fig. 7. The spectra shown are inverted second derivative spectra of the δCH_2 (1450–1480 cm^{-1}) and δCD_2 spectral regions (1080–1100 cm^{-1}). It is interesting to note the absence of splitting in the δCH_2 (1469 cm^{-1}) band, which is observed for all four ceramides. In contrast, the δCD_2 band is quite clearly split in the spectra of d_{39}C20-Cer (also for d_{31}C16-Cer and d_{35}C18-Cer, not shown) although not in d_{27}C14-Cer. The d_{27}C14-Cer derivative exhibits a 0.6 cm^{-1} increase at the solid-solid phase transition temperature while the scissoring doublet of d_{39}C20-Cer collapses at 70°C. The latter observation is consistent with an orthorhombic → hexagonal transition.

Spectral features arising from the polar regions of these synthetic ceramides are, as expected, unaffected by isotopic labeling of the fatty acid chain. Thus identical behavior was observed for fully proteated and isotopically labeled molecules. For brevity, only spectra from C14-Cer and C20-Cer in ^2H_2O buffer are plotted in Fig. 8. Analogous behavior is observed for C16-Cer and C18-Cer. The headgroup amide I ($\nu C=O$) and II (mixed νC-N and δN-H) modes are both split into two components. The amide I peaks appear at approx. 1615 and 1645 cm^{-1} while the amide II bands are at approx. 1545 and 1567 cm^{-1}. The disappearance of the amide II band occurs at approx. 65°C for C14-Cer (and C16-Cer, not shown) and at approx. 67°C for C20-Cer (and C18-Cer, not shown). This is the temperature at which the orthorhombic-hexagonal chain packing transition occurs for these molecules (see Fig. 2). However, there is a small amide II band (approx. 1550 cm^{-1}) remaining in the spectra of C20-Cer (and C18-Cer, not shown) until the onset of the major chain melting transition.

The presence of the 4,5 *trans* C=C bond near the headgroup of ceramide 2 likely has a significant impact on both the headgroup and base chain conformational freedom of this molecule. As in our previous studies of fatty acid heterogenous ceramide 2, at least two bands appear to come from the out-of-plane bending mode of the vinylic C-H [21]. In Fig. 9 the 940–1000 cm^{-1} spectral region is displayed for C14-Cer and C20-Cer as a function of temperature. Both molecules have bands at 960 and 980 cm^{-1} at lower temperatures (as do C16-Cer and C18-Cer, not shown), while C14-Cer (and C16-Cer, not shown) has an additional band at 970 cm^{-1}. Above the solid-solid transition temperature, coincident with changes in the amide I and II modes, the 980 band shifts to 985 cm^{-1}, the 970 cm^{-1} mode disappears, and the 960 cm^{-1} remains. In all cases the 960 and 985 cm^{-1} bands persist until complete chain melting at 90°C, at which point the two peaks collapse to a single peak at 970 cm^{-1}. This behavior, which arises from the proteated base chains, is identical for the corresponding deuterated ceramides, as expected.

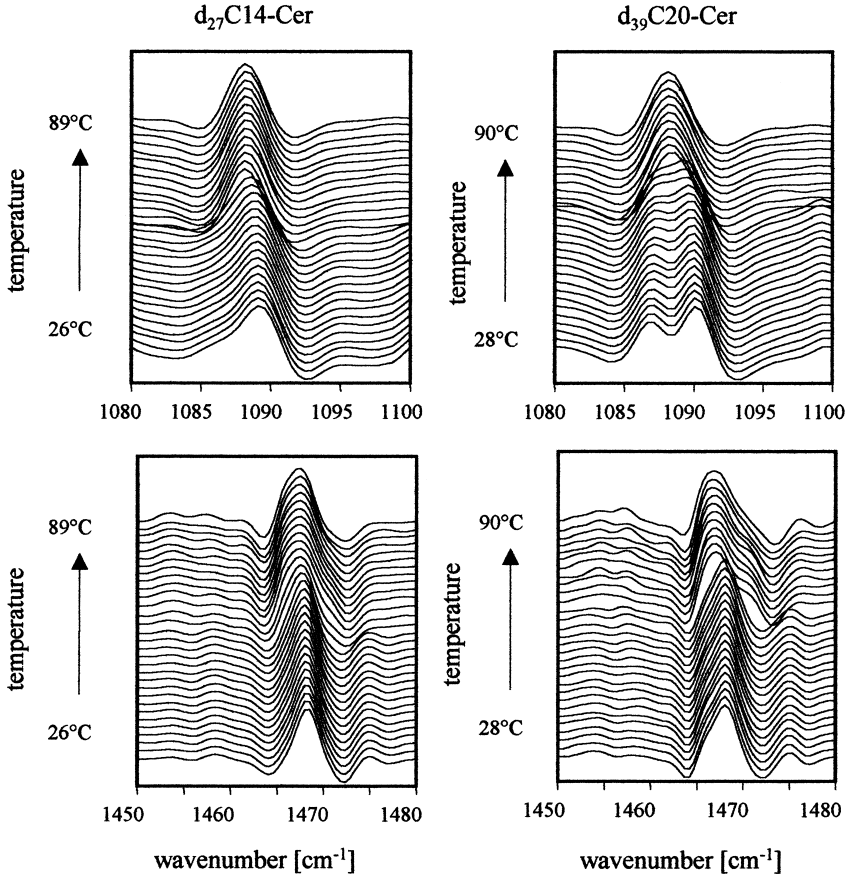

Fig. 7. Inverted second derivative spectra of d_{27}C14-Cer and d_{39}C20-Cer showing the δCD_2 (1080–1100 cm^{-1}, fatty acid chain) and δCH_2 (1450–1480 cm^{-1}, base chain) spectral regions as a function of temperature. Note the absence of splitting due to absence of domains in the base chain modes in each case.

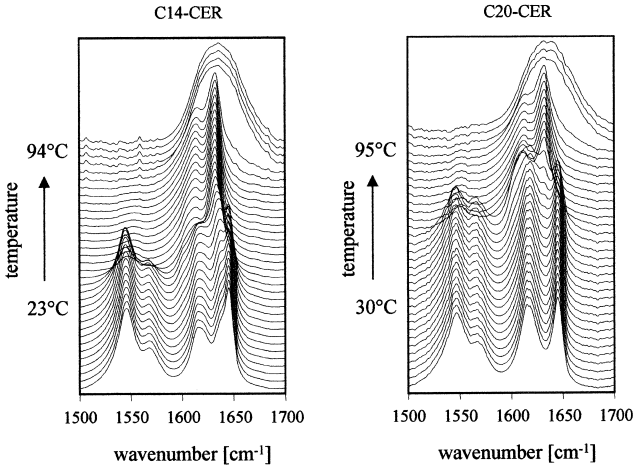

Fig. 8. Original spectra of C14-Cer and C20-Cer in ^2H_2O, showing the splitting of both the amide I (approx. 1650 cm^{-1}) and amide II (approx. 1550 cm^{-1}) modes as a function of temperature. At higher temperature the amide II mode disappears in both cases due to H-D exchange.

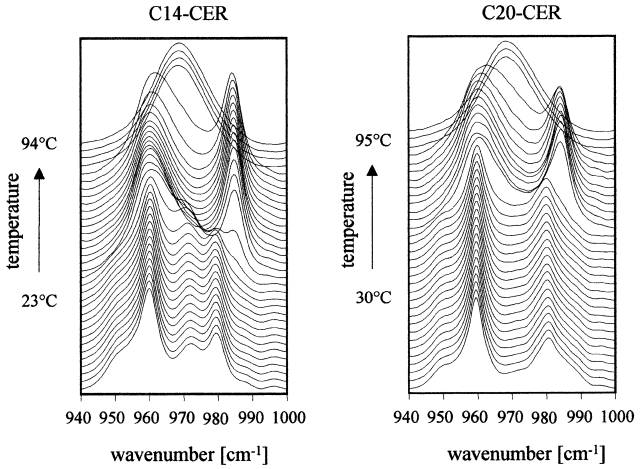

Fig. 9. Original spectra of the out-of-plane HC=C region (940–1000 cm^{-1}) of C14-Cer and C20-Cer in ^2H_2O as a function of temperature.

4. Discussion

The use of IR spectroscopy combined with isotopic labeling provides unique information about molecular structure and interactions in this set of chain length homogeneous ceramide molecules. Previous studies of this class of molecules have utilized samples possessing substantial heterogeneity in the fatty acid chain, thereby limiting the information available from particular molecular species.

DSC provides a convenient characterization of the thermodynamics of phase transitions. The transition temperatures observed for all the ceramide derivatives were essentially chain length independent, with the slight exception of C14-Cer, with a T_m consistently approx. 6°C lower than the other three molecules. It is interesting to note that when the ceramides were hydrated from the dried powder as opposed to a film that the T_m of C14-Cer was within 1–2°C of the other ceramides. Overall, the uncertainty in the DSC measurements is on the order of ± 1°C. This reduced dependence of T_m on fatty acid chain length is in contrast to the vast body of data for hydrated phospholipid bilayers. For example, the members of a comparable fully hydrated series of phosphatidylcholines (PCs), 1-myristoyl, 2-stearoylPC, 1-palmitoyl, 2-stearoylPC, and 1,2-disteroylPC, exhibit main transition temperatures of 42, 47.5 and 55°C, respectively [27]. Similar effects are noted for other lipid classes where one chain length is held constant and the second chain length is systematically varied [28].

While DSC provides thermodynamic data concerning the phase behavior of hydrated lipids it obviously does not provide any molecular information, FTIR spectroscopy provides molecular level detail about the observed phase transitions. The methylene stretching mode frequency for each of the four ceramides are plotted in Fig. 2. In general, this mode is sensitive to both chain conformation and altered chain packing [29,30]. Frequencies above approx. 2852 cm^{-1} are indicative of chains with a substantial fraction of disorder. However, the observation of $\nu_s CH_2$ frequencies below 2850 cm^{-1} at low temperatures indicate that the ceramide chains are in the all-*trans* conformation. Therefore, the transition observed near 70°C at approx. 2848 cm^{-1} results from altered chain packing of ordered ceramide chains (for further details about the effects of conformations vs. packing changes on methylene frequencies, see the discussion in [20,21]). Thus the lower temperature discontinuity evident for C18-Cer and C20-Cer is assigned to a solid-solid phase transition. As noted above, this transition is only marginally detectable for the C14- and C16-ceramides. The straightforward interpretation of these data would be that there is significantly more rearrangement in the chain packing of the longer chain ceramides. However, utilizing the isotopically labeled ceramides, and probing the inter- and intramolecular behavior of the individual ceramide chains, leads to a different conclusion. The methylene stretching modes ($\nu_s CH_2$ and $\nu_s CD_2$) plotted in Fig. 3 for the base chain and fatty acid chain, respectively, reveal significant frequency changes at approx. 65°C for both C14-Cer and C16-Cer. Thus, while $\nu_s CH_2$ increases by 1 cm^{-1} (notable in both derivatives), $\nu_s CD_2$ decreases by >1 cm^{-1} (notable mainly in the C14 derivative) suggesting a structural alteration for these molecules in which packing becomes tighter (more restricted) for the fatty acid chains and looser for the base chains. This information was obviously not available from the data in Fig. 2. In that instance, the average behavior of the C14-Cer and C16-Cer chains was measured. Thus, no change in chain packing could be detected for these ceramides, presumably due to the fact that $\nu_s CH_2$ of the base chain was increasing while $\nu_s CH_2$ of the fatty acid chain was decreasing, resulting in no net change in $\nu_s CH_2$.

The current FTIR spectroscopy measurements also provide specific information about ceramide chain packing. This is accomplished through examination of the methylene bending modes which are particularly well suited for detection of domains of orthorhombic subcell structure [25]. When conformationally ordered chains are packed in an orthorhombic subcell arrangement, the scissoring modes split into a doublet [31]. This phenomenon has been exploited in many studies by Snyder and his colleagues to monitor the kinetics of demixing events in alkanes [32], and structural organization in phospholipid domains [33]. Our laboratories have used these modes to investigate ordered lipid phases in stratum corneum skin barrier models [20,22]. Some of the primary data are presented in Fig. 6 and show the temper-

ature dependence of the methylene scissoring vibrations for C14-Cer and C20-Cer. The narrower peak for the C14-Cer suggests hexagonal packing, whereas the broad nature of the δCH_2 peak for the C20-Cer suggests the presence of splitting in the underlying modes. The presence of a looser packing for the C14-Cer is also manifest in Fig. 4B, where the linewidths of the CH_2 stretching vibrations of the proteated base chain for d_{27}C14-Cer are substantially (15–30%) greater than for the other derivatives. This looser packing is reflected in the reduced interchain vibrational coupling (or, in fact, absence of the orthorhombic perpendicular phase) in the fully proteated species, as shown through the scissoring modes in Fig. 6.

The utility of isotopic substitution for revealing intermolecular behavior is illustrated by the scissoring mode spectra of the fatty acid and base chains for d_{27}C14-Cer and d_{39}C20-Cer in Fig. 7. In the d_{27}C14-Cer both the δCH_2 and δCD_2 of the sphingosine and fatty acid chains, respectively, exhibit a single narrow peak, characteristic of hexagonal chain packing. The spectra show little variation with temperature, although a slight frequency shift is observed for both modes at the first transition (approx. 65°C, as determined from Fig. 2).

The δCD_2 of the deuterated fatty acid chains in d_{39}C20-Cer exhibit a 3 cm^{-1} splitting at all temperatures below the orthorhombic-hexagonal chain packing transition (this is also observed for d_{35}C16-Cer and d_{37}C18-Cer). At the first transition (as determined from $\nu_s CH_2$ in Fig. 2), the splitting collapses and a single peak is observed at 1087 cm^{-1}. This observation provides direct evidence that the deuterated chains are vibrationally coupled in microdomains, at lower temperatures. The segregation of microdomains (i.e., 3–5 chains) has also been reported by Levin and co-workers in studies of gel phase phospholipids [34]. Interestingly, the δCH_2 of the d_{39}C20-Cer sphingosine (proteated) base chain exhibits a sharp single scissoring band at all temperatures (see Fig. 7). This lack of splitting implies the base chains in these orthorhombically packed assemblies are sufficiently separated so as to inhibit vibrational coupling between them.

Quantitative evaluation of the band contour in the deuterated derivatives permits the detection of microdomains ranging from one to 100 chains. The method, developed by Snyder and his co-workers, is based on studies of mixtures of molecules with differing isotopes (or of individual molecules containing isotopically mixed chains). As noted above, the components of the scissoring modes appear at approx. 1462–1474 cm^{-1} for proteated chains, and 1084–1092 cm^{-1} for deuterated chains, in pure phases of molecules with orthorhombic perpendicular subcell packing. Snyder et al. have shown that the splitting increases with domain size and asymptotically approaches a maximum value (approx. 12 cm^{-1} for CH_2 and 8 cm^{-1} for CD_2) for domains larger than about 100 chains [35]. Thus the band shape reflects the domain size distribution function. For C20-Cer the splitting is reduced from the maximum for two reasons. First, each deuterated chain has a proteated chain adjacent to it. Second, the domains of deuterated chains are relatively small. Comparison of the magnitude of the CD_2 scissoring splitting with the calculated curves of Snyder et al., suggests a domain size of 3–5 chains, although the effect of a constant proteated chain in the vicinity of a deuterated chain on the scissoring contour is difficult to account for precisely.

IR offers the ability to directly monitor water penetration into the lamellae as revealed by examination of the temperature dependence of the amide II vibration (approx. 1550 cm^{-1}) intensity (Fig. 8). This normal mode is a mixture of C-N stretch and N-H in-plane bending internal coordinates. $H \rightarrow D$ exchange alters the mixing of internal coordinates and lowers the frequency to approx. 1450 cm^{-1}. At temperatures well below the orthorhombic-hexagonal chain packing transition, the relative intensity of the amide II mode is constant, thus indicating that ^2H_2O is unable to penetrate into the highly ordered lamellar structure. In contrast, the band intensity diminishes greatly near the orthorhombic-hexagonal chain packing transition, the direct result of the $H \rightarrow D$ exchange shifting the amide II frequency. We have previously observed that in bovine brain ceramide each of the amide I and II modes are split into a doublet [21]. This splitting was tentatively attributed to intermolecular interactions between amide groups located in different layers in the structure, a hypothesis supported by recent ceramide 2 monolayer studies in which amide I splitting was not observed in conformationally ordered monolayers [24]. It might be ex-

pected that if there were substantial interlamellar water, the intermolecular interaction, which is a relatively short range interaction, would be lost.

Thus, we propose the following sequence of thermotropic events for these molecules. Hydration of the headgroup region (as shown from the disappearance of the amide II mode) is accompanied by a solid-solid phase transition (orthorhombic-to-hexagonal, at least for the C16, C18 and C20 derivatives). The hydration is limited to at most a few water molecules, resulting in a diminished chain length dependence of the chain melting transition temperature compared to well hydrated systems such as PCs. Cevc and Marsh, who proposed equations for the chain length dependence of the transition temperature of anhydrous phospholipids, and for the hydration-induced transition-temperature shifts, have discussed the latter effect in detail [36]. We cannot apply these equations to the ceramide series studied here, since we do not know the exact hydration levels although we suspect these may be different for each derivative.

The suggestion of limited ceramide hydration, even under conditions of the ATR experiments reported here (sample submerged under ^2H_2O) is consistent with the X-ray measurements of Bouwstra and colleagues, who observed no change in interlamellar spacing as a function of increased water content in studies of hydrated SC lipids [37]. Similar findings were recently reported by McIntosh and colleagues in X-ray studies of galactosylceramides [38]. Finally, Shipley and co-workers used DSC to study the effect of putative hydration (i.e. percent water content in a ceramide sample) on transition temperatures of C16-Cer [39]. A 4° decrease in T_m (compared to the anhydrous lipid) was noted for a sample containing 3.6 wt% water (approx. one water molecule/lipid molecule). However, little further decrease in T_m was observed with additional water, suggesting that further penetration into the lamellae to increase the C16-Cer hydration level was limited.

4.1. Implications for the role of ceramide 2 in skin barrier function

The primary motivation for these biophysical studies is to acquire precise molecular level understanding of the inter- and intramolecular organization and phase behavior of hydrated ceramide 2 molecules. This is because ceramide 2 is a major constituent of the SC lipid matrix and therefore plays a critical role in skin barrier function. It is hoped that this understanding will provide some insight into the specific molecular contribution that ceramide 2 makes to SC lipid organization and barrier function.

It is interesting to note that ceramide 2 isolated from human stratum corneum generally contains longer chain fatty acids than those utilized in the current study [6]. However, the current work indicates that the fundamental phase behavior of ceramide 2 may be nearly independent of chain length, primarily, due to its very small sphere of hydration (it is also worth noting that splitting of the headgroup amide I and II modes, is also independent of chain length). One would expect, however, that mixing (and demixing) in multicomponent lamellar systems will be significantly influenced by the chain length of the various components. With this understanding of the phase behavior of these fatty acid homogeneous ceramide 2 molecules we are now investigating multicomponent models of the skin barrier lipid matrix.

Acknowledgements

This work was supported in part by a Public Health Service grant (GM 29864) to RM. We thank Dr. Jenifer Thewalt, Simon Fraser University, for providing the first synthetic ceramide 2 samples.

References

[1] H. Schaefer, T.E. Redelmeier, Skin Barrier: Principles of Percutaneous Absorption, Karger, Basel, 1996.
[2] B. Forslind, Thromb. Res. 80 (1995) 1–22.
[3] P.M. Elias, J. Control. Release 15 (1991) 199–208.
[4] P.W. Wertz, B. van den Bergh, Chem. Phys. Lipids 91 (1998) 85–96.
[5] A.V. Rawlings, in: R. Hamilton, W. Christie (Eds.), Waxes, The Oily Press, Dundee, 1995, pp. 223–256.
[6] P.W. Wertz, M.C. Miethke, S.A. Long, J.S. Strauss, D.T. Downing, J. Invest. Dermatol. 84 (1985) 410–412.
[7] L. Norlen, I. Nicander, A. Lundsjo, T. Cronholm, B. Forslind, Arch. Dermatol. Res. 290 (1998) 508–516.
[8] K.J. Robson, M.E. Stewart, S. Michelsen, N.D. Lazo, D.T. Downing, J. Lipid Res. 35 (1994) 2060–2068.

[9] R. White, M. Walker, Biochem. Soc. Trans. 18 (1990) 881–882.
[10] C.-H. Han, R. Sanftleben, T.S. Wiedmann, Lipids 30 (1995) 121–128.
[11] G.M. Golden, D.B. Guzek, R.R. Harris, J.E. McKie, R.O. Potts, J. Invest. Dermatol. 86 (1986) 222–259.
[12] T.J. McIntosh, M.E. Stewart, D.T. Downing, Biochemistry 35 (1996) 3649–3653.
[13] J.A. Bouwstra, J. Thewalt, G.S. Gooris, N. Kitson, Biochemistry 36 (1997) 7717–7725.
[14] J.A. Bouwstra, G.S. Gooris, K. Cheng, A. Weerheim, W. Bras, M. Ponec, J. Lipid Res. 37 (1996) 999–1011.
[15] D.T. Parrott, J.E. Turner, Biochim. Biophys. Acta 1147 (1993) 273–276.
[16] N. Kitson, J. Thewalt, M. Lafleur, M. Bloom, Biochemistry 33 (1994) 6707–6715.
[17] J. Thewalt, N. Kitson, C. Araujo, A. MacKay, M. Bloom, Biochem. Biophys. Res. Commun. 188 (1992) 1247–1252.
[18] D.B. Fenske, J.L. Thewalt, M. Bloom, N. Kitson, Biophys. J. 67 (1994) 1562–1573.
[19] W. Abraham, D.T. Downing, Pharm. Res. 9 (1992) 1415–1421.
[20] D.J. Moore, M.E. Rerek, R. Mendelsohn, Biochem. Biophys. Res. Commun. 231 (1997) 797–801.
[21] D.J. Moore, M.E. Rerek, R. Mendelsohn, J. Phys. Chem. B 101 (1997) 8933–8940.
[22] D.J. Moore, M.E. Rerek, R. Mendelsohn, Int. J. Cosmet. Sci. 21 (1999) 353–368.
[23] R. Mendelsohn, D.J. Moore, in: Y.A. Hannun, A.H. Merrill (Eds.), Sphingolipid Metabolsim and Cell Signaling, vol. 312, Academic Press, New York, 2000.
[24] C.R. Flach, R. Mendelsohn, M.E. Rerek, D.J. Moore, J. Phys. Chem. 104 (2000) 2159–2165.
[25] R.G. Snyder, J. Mol. Spectrosc. 7 (1961) 116–144.
[26] R. Mendelsohn, D.J. Moore, Chem. Phys. Lipids 96 (1998) 141–157.
[27] R. Koynova, M. Caffrey, Biochim. Biophys. Acta 1376 (1998) 91–145.
[28] D.M. Small, The Physical Chemistry of Lipids: from Alkanes to Phospholipids, vol. 4, Plenum Press, New York, 1986.
[29] R.G. Snyder, H.L. Strauss, C.A. Elliger, J. Phys. Chem. 86 (1982) 5145–5150.
[30] R.A. MacPhail, H.L. Strauss, R.G. Snyder, C.A. Ellinger, J. Phys. Chem. 88 (1984) 334–341.
[31] R.G. Snyder, J. Chem. Phys. 71 (1979) 3229–3235.
[32] R.G. Snyder, M.C. Goh, V.J.P. Srivatsavoy, H.L. Strauss, D.L. Dorset, J. Phys. Chem. 96 (1992) 10008–10019.
[33] R. Mendelsohn, G.L. Liang, H.L. Strauss, R.G. Snyder, Biophys. J. 69 (1996) 1987–1998.
[34] H. Wang, P.K. McCarthy, B.J. Litman, I.W. Levin, Biophys. J. 76 (1999) A58.
[35] R. Mendelsohn, R.G. Snyder, in: K.M. Merz, B. Roux (Eds.), Biological Membranes: a Molecular Perspective from Computation and Experiment, Birkhauser, Boston, MA, 1996, pp. 145–174.
[36] G. Cevc, D. Marsh, Phospholipid Bilayers: Physical Principles and Models, Wiley-Interscience, New York, 1987.
[37] J.A. Bouwstra, G.S. Gooris, M.A. Salomons-de Vries, J.A. van der Spek, W. Bras, Int. J. Pharm. 84 (1992) 205–216.
[38] K. Kulkarni, D.S. Snyder, T.J. McIntosh, Biochemistry 38 (1999) 15264–15271.
[39] J. Shah, J.M. Atienza, R.I. Duclos, A.V. Rawlings, Z. Dong, G.G. Shipley, J. Lipid Res. 36 (1995) 1936–1944.